Available online at www.sciencedirect.com

SciVerse ScienceDirect

Ceramics International 38 (2012) 5843–5851

CERAMICS INTERNATIONAL

www.elsevier.com/locate/ceramint

Effect of mixed solvent on structural, morphological, and optoelectrical properties of spin-coated TiO_2 thin films

Mohammad Reza Golobostanfard *, Hossein Abdizadeh

School of Metallurgy & Materials Engineering, College of Engineering, University of Tehran, P.O. Box: 14395-553, Tehran, Iran

Received 15 February 2012; received in revised form 10 April 2012; accepted 11 April 2012
Available online 19 April 2012

Abstract

Nanocrystalline TiO_2 anatase thin films have been synthesized from alkoxide solution via sol–gel spin coating method. The effects of different solvents of methanol, ethanol, 1-propanol, 2-propanol, 1-butanol, 2-butanol, and tert-butanol as well as those of mixed solvents on crystal structure, thermal behavior, morphology, and optoelectrical properties were investigated. It was found that not only the occurrence of rutile with anatase phase was solvent dependent, but also the morphology and optoelectrical properties of the films were strongly affected by solvent type. However, using two different types of alcohols as a single solvent brings the advantages of both solvents. Also, some unique properties in mixed solvent samples could be achieved. The viscosity, gel time, boiling point, possible complexes, dipole moment, and chain length of the solvent affect the packing density, lattice distortion, interfaces, thickness, optical band gap, refractive index, and extinction coefficient.

Keywords: TiO_2; Sol–gel processes; Films; Optical properties

1. Introduction

In recent years, TiO_2 has been widely used in many different applications such as photocatalysts [1], solar cells [2,3], gas sensors [4], and electrochromic devices [5] due to its good transmittance in visible region (>80%), high refractive index (2.488 for anatase and 2.7 for rutile phase in bulk form), chemical stability, wide and tunable band gap (3.2 eV for anatase and 3 eV for rutile), and long term photostability [6–10]. TiO_2 exists in three crystalline phases of rutile (tetragonal, $P4_2/mmm$), anatase (tetragonal, $I4_1/amd$), and brookite (orthorhombic, Pbca) at ambient temperatures and pressures, among which the rutile is the most stable phase. Rutile has smaller electron effective mass, higher density, and higher refractive index than anatase. However, the anatase has very shallow donor level, high electron mobility and trap controlled electronic conduction. According to these properties, the latter is preferred in most optoelectronic and photocatalyst applications but the former used in protective coatings [11,12].

The structural, optical, and electrical properties of TiO_2 thin films strongly depend on the deposition method. TiO_2 thin films have been prepared by different methods such as electron beam evaporation [13], ion beam assisted deposition [14], DC and RF reactive magnetron sputtering [15], sol–gel method [16–18], molecular beam epitaxy [19], chemical vapor deposition [20], electrodeposition [21], pulsed laser deposition [22], and spray pyrolysis [23]. Among the mentioned methods, sol–gel method has the advantages of simplicity, inexpensiveness, low temperature processing, the ability to form homogeneous multicomponent films on large areas, non-vacuum processing, possibility to form porous film, and customizable microstructure [24].

Different solvents in sol–gel method could extremely affect the crystalline phase, microstructure, optoelectrical properties of the films due to the different boiling points, chain lengths and structure, possible complexes, coordination numbers, and polarity of the solvents. Although, the effect of solvent on sol–gel behavior of TiO_2 sol has been performed before [25], but effect of mixed solvent as well as individual solvent with different chain lengths and molecule structures on TiO_2 sol was never carried out. So, in this article the effect of methanol, ethanol, 1-propanol, 2-propanol, 1-butanol, 2-butanol and tert-butanol on structure, morphology, and optoelectronic properties

* Corresponding author. Tel.: +98 9122300382; fax: +98 21 88006076.
E-mail address: Bostanfr@ut.ac.ir (M.R. Golobostanfard).

0272-8842/$36.00
http://dx.doi.org/10.1016/j.ceramint.2012.04.034

of TiO_2 transparent nanostructured thin films synthesized via sol–gel spin coating method was investigated separately and in mixed state of solvents.

2. Experimental

2.1. Materials

All chemicals including methanol (MeOH, analytical reagent grade), ethanol (EtOH, synthetic grade), 1-propanol (1PrOH, analytical reagent grade), 2-propanol (2PrOH, analytical reagent grade), 1-butanol (1BuOH, analytical reagent grade), 2-butanol (2BuOH, analytical reagent grade), tert-butanol (tBuOH, analytical reagent grade), nitric acid (HNO_3, 65%), and titanium tetra isopropoxide (TTiP, 99%) were obtained from Merck chemicals. In all samples deionized water (DIW, 18.2 MΩ) was used.

2.2. Film preparation

In order to achieve a transparent and high quality thin film, the transparent and stable sol is required. For this purpose, partial condensation and hydrolysis of TTiP with DIW was controlled by controlling the proportion of TTiP, solvent, DIW, and HNO_3. It was found that the most stable sol resulting in a high quality film obtained in TTiP:DIW:HNO_3 molar ratio of 1:4:0.5 in constant solvent volume (0.17 M). TTiP was dissolved in each solvent and stirred for 30 min in closed container. For preparation of the sol, the solution of DIW, solvent, and HNO_3, which stirred for 10 min, were added drop wisely to the TTiP solution under vigorous stirring. The solution was stirred at room temperature in air atmosphere for 1 h to complete the hydrolysis and condensation and reach the transparent sol. In order to investigate the effect of each solvent on structure and properties of the films, different solvents of MeOH, EtOH, 1PrOH, 2PrOH, 1BuOH, 2BuOH and tBuOH individually and also in mixed form (in equal amount) were examined. Table 1 shows the physical properties of individual solvents. The sol behaviors of individual and mixed solvent samples are brought together in Table 2. In all cases, while the solvent was changed, the amounts of other sol components were held constant.

The soda lime glass substrates were cleaned with detergent, EtOH, and DIW in an ultrasonic bath and dried with stream of hot air prior to use. Thin films of TiO_2 were deposited by spin coating method using a spin coater (Model VMC409, Nanotajhiz Pasargad). The films were spin coated at a spin rate of 3000 rpm for 30 s under low vacuum and dried for 2 min at room temperature and 10 min at 100 °C. The cycles of spin coating and drying were repeated 10 times to achieve desired thickness. Finally, the films were calcined at 450 °C for 1 h with the rate of 5 °C/min.

In this article the DIW content was chosen in the maximum and critical amount to increase the reactions and avoid any unexpected complexes. Higher water content (DIW/TTiP ratio more than 4) causes fast precipitation or low sol stability. On the other hand, lower water content (DIW/TTiP ratio less than 4) forms different types of complexes. As a catalyst, the HNO_3 was used instead of HCl, which promote the formation of rutile. Inhibition effect of mixed solvent on formation of this unwanted phase might be advantageous.

2.3. Characterization

The phase structure of the films and obtained powders from the remaining sols was studied by X-ray diffraction method (XRD, Philips X-pert pro PW1730, 40 kV, 30 mA, Cu-K_α, $\lambda = 1.54056$ Å) in the range of 20–80°. The morphologies of the resultant samples were observed by field emission scanning electron microscope (FESEM, Hitachi S4160). The thermal analysis of the samples were performed on DSC/TG (Netzsch, STA409) in the range of 25–1000 °C at 10 °C/min under air atmosphere. The optical transmittance spectra were recorded in the wavelength range of 200–1000 nm (UV–vis spectroscopy, PG instrument T80+ spectrophotometer). The thickness of the films were determined from a FESEM cross-sectional image and also calculated from optical data with envelope method.

3. Results and discussion

All the sols except 2PrOH, 2BuOH and tBuOH show very good stability and gel time of about more than 2 days in open container and of about one month in closed container. The sol stability, gel transparency, and gel time of all samples are brought together in Table 2. The gel time could be described by the boiling point, chain length, and the possible complexes of the solvents. 1PrOH and 1BuOH solvents prepared the most stable sols due to the higher order complexes, higher boiling points, and lower dipole moments than MeOH, EtOH, and 2PrOH. Although the boiling point of 2BuOH is comparable with 1PrOH, the viscosity is much higher and dipole moment is much lower than 1PrOH which affect the gel time of this sample. On the other hand, both boiling point and dipole moment of this solvent are much lower than that of 1BuOH

Table 1
Physical properties of individual solvents.

Solvent	Boiling point (°C)	Molar mass (g/mol)	Density (g/cm^3)	Viscosity at 25 °C (Pa s)	Dipole moment (Debye)	Dielectric constant at 20 °C
MeOH	65	32.04	0.7918	0.59×10^{-3}	1.69	32.35
EtOH	78	46.07	0.7890	1.20×10^{-3}	1.69	25.00
1PrOH	98	60.10	0.8034	1.94×10^{-3}	1.68	20.81
2PrOH	82	60.10	0.7860	1.96×10^{-3}	1.66	18.62
1BuOH	118	74.12	0.8105	3.00×10^{-3}	1.66	17.80
2BuOH	99	74.12	0.8063	3.40×10^{-3}	1.52	15.80

Table 2
Sol stability, gel transparency, and gel time of the samples.

Sample	Sol stability[a]	Gel transparency	Gel time	Crystallite size (nm)
MeOH	4	Transparent	3 days	58 ± 12
EtOH	5	Transparent	2 days	24 ± 5
1PrOH	2	Transparent	10 days	19 ± 5
2PrOH	9	Translucent	4 h	14 ± 5
1BuOH	1	Transparent	1 month	22 ± 5
2BuOH	10	Opaque	During	19 ± 5
tBuOH	9	Opaque	2 h	25 ± 5
EtOH/2PrOH	6	Opaque	1 day	12 ± 6
MeOH/2PrOH	5	Opaque	2 days	10 ± 6
MeOH/1PrOH	4	Translucent	5 days[b]	136 ± 14
MeOH/EtOH	4	Transparent	3 days	11 ± 6
1PrOH/2PrOH	3	Opaque	6 days	31 ± 6
EtOH/1PrOH	2	Transparent	8 days	12 ± 6

[a] 1: Unbelievable; 2: amazing; 3: great; 4: good; 5: above average; 6: average; 7: below average; 8: bad; 9: weak; and 10: terrible.
[b] After 2 days converted to the milky sol and after 3 days formed the gel.

which causes lower gel time. Moreover, the steric hindrance of 2-butoxy is lower than 1-butoxy ligands. In mixed solvent samples, EtOH/2PrOH, MeOH/2PrOH and 1PrOH/2PrOH samples which contain 2PrOH as a one component, monomeric oligomers with low hindrance and fast hydrolysis reaction was formed due to the similarity of this solvent with TTiP ligands, which resulted in the very fast gel time and quite unstable sol. However, in these sols compared to the 2PrOH sample, the gel time promoted by means of other solvents and increased in the order of EtOH < MeOH < 1PrOH. This trend is completely matched with gel time trend of these solvents individually. On the other hand, in MeOH/1PrOH, MeOH/EtOH, and EtOH/1PrOH complicated complexes were formed which due to the steric hindrance, the gel time postponed to the very longer time. The gel time in EtOH/1PrOH was the longest among mixed solvent samples which is caused by the existence of EtOH and 1PrOH with higher boiling point than MeOH. Scheme 1 shows schematically the contoured gel times of the samples.

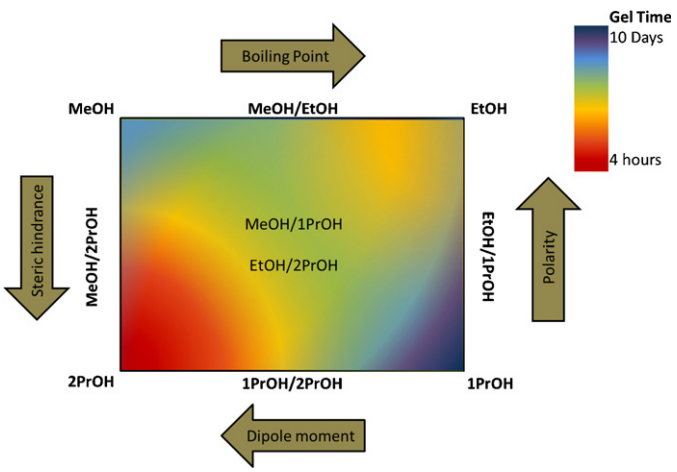

Scheme 1. Schematic representation of the gel time for all samples.

3.1. XRD analysis

XRD patterns of powders with different solvents of MeOH, EtOH, 1PrOH, 2PrOH, 2BuOH calcined at 450 °C are shown in Fig. 1. It could be seen that the anatase phase (JCPDS 21-1272) [26] formed in all samples as the major crystalline phase, while the rutile phase (JCPDS 21-1276) [27] crystallized only in EtOH and 1PrOH samples as minor phase beside anatase (anatase is more stable thermodynamically in smaller particles [28]). It is believed that the alcohol coordination number could efficiently affect the resulted oligomers and hence the structure of building blocks. As a result, 5-fold coordinated titanium and 2- and 3-fold coordinated oxygen in (1 0 0) plane of rutile is formed instead of 5-fold coordinated titanium and 2-fold coordinated oxygen in (1 0 1) plane of anatase in some solvents [28].

The crystallite size was calculated using full width at half maximum (FWHM) of the intense diffraction peak of anatase TiO_2 (1 0 1) according to Scherer equation $D = (0.89 \times \lambda)/\beta \cos\theta$, where D is the crystallite size in nm, λ is the wavelength of incident X-ray in nm, θ is Bragg angle, and β is FWHM in radians [29]. The measured crystallite sizes for the xerogel powders after calcination for each sample are given in Table 2.

The XRD pattern of powder samples with mixed solvent of EtOH/2PrOH, MeOH/2PrOH, MeOH/1PrOH, MeOH/EtOH, 1PrOH/2PrOH, and EtOH/1PrOH are presented in Fig. 2. Very slight formation of rutile phase in EtOH/2PrOH sample could be detected. However, in all other samples, the anatase TiO_2 formed as the only crystalline phase, which shows that using mixed solvent reduces the formation of rutile. Nevertheless, the reduction in crystallization of the MeOH/1PrOH, MeOH/EtOH, and 1PrOH/2PrOH could be observed.

The lattice parameters of tetragonal anatase phase (a and c) could be calculated using relations $a = b = 2 \times d_{2\,0\,0}$ and $c = 4 \times d_{0\,0\,4}$. These parameters for all samples are shown in Fig. 3. It could be seen that in most cases, the a parameter is very close to the reported bulk values of anatase (a = 3.7852 Å),

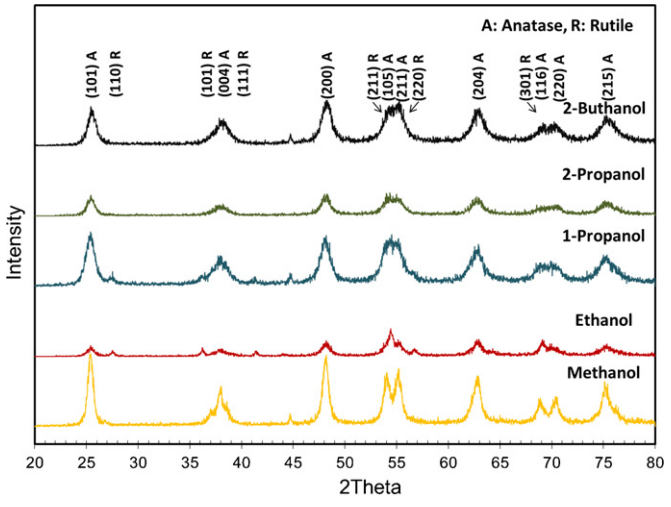

Fig. 1. XRD patterns of MeOH, EtOH, 1PrOH, 2PrOH, and 2BuOH powders calcined at 450 °C.

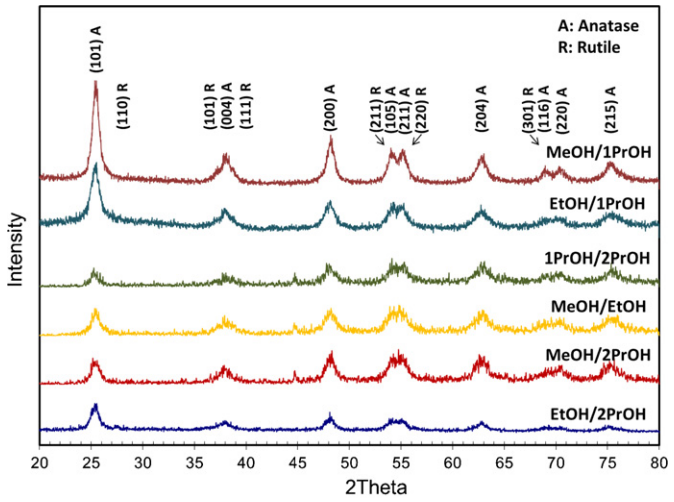

Fig. 2. XRD patterns of EtOH/2PrOH, MeOH/2PrOH, MeOH/EtOH, 1PrOH/2PrOH, EtOH, 1PrOH, and MeOH/1PrOH powders calcined at 450 °C.

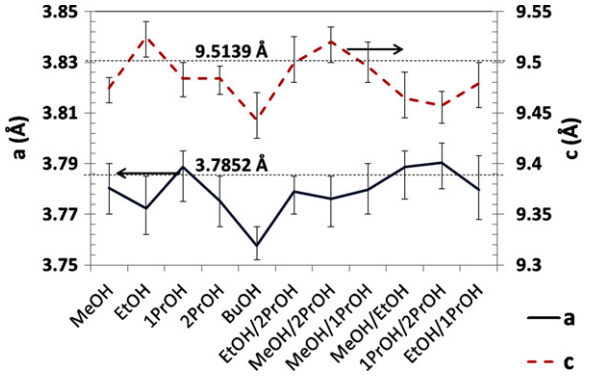

Fig. 3. Lattice parameters of a and c for all samples. The dashed lines show the exact values of a and c for anatase TiO_2.

but c values show slightly difference from the bulk value ($c = 9.5139$ Å) [26] and dependence to the solvent type.

3.2. FESEM micrographs

Sols with 2PrOH, 2BuOH and tBuOH are not suitable for film preparation due to the low sol stability. The FESEM images for the films with solvents of MeOH, EtOH, and 1PrOH after calcination are shown in Fig. 4. MeOH, EtOH, and 1PrOH films were formed with a very high surface quality showing particles with mean size of about 25, 14, and 18 nm, respectively. The particle size increases with solvent as in the order of EtOH < 1PrOH < MeOH. Better crystallization behavior of MeOH, confirmed by the XRD results, may cause an increase in grain size. Also, existence of very low amount of water in MeOH causes fast hydrolysis which was peptized by acid addition in this sample. In Fig. 4d, the cross section SEM micrograph for 10-layer film of 1PrOH sample is shown. The thickness of this film is about 460 nm.

Fig. 5 shows the FESEM micrographs of EtOH/2PrOH, MeOH/2PrOH, MeOH/1PrOH, MeOH/EtOH, 1PrOH/2PrOH, and EtOH/1PrOH. In all films very dense structure with some pores could be observed due to the shrinkage during calcination. The mean particle size of less than 25 nm could be seen except for the MeOH/1PrOH film which formed a slightly different microstructure. It could be seen from Table 2 that although the sol stability for this sample is good, after two days it converts to milky sol, which is the sign of large particle formation. This phenomenon happens very fast during film preparation and causes formation of larger particles on the film. In sols containing 2PrOH, some lighter spots in some regions of the film could be seen which may be due to the higher hydrolysis of these samples.

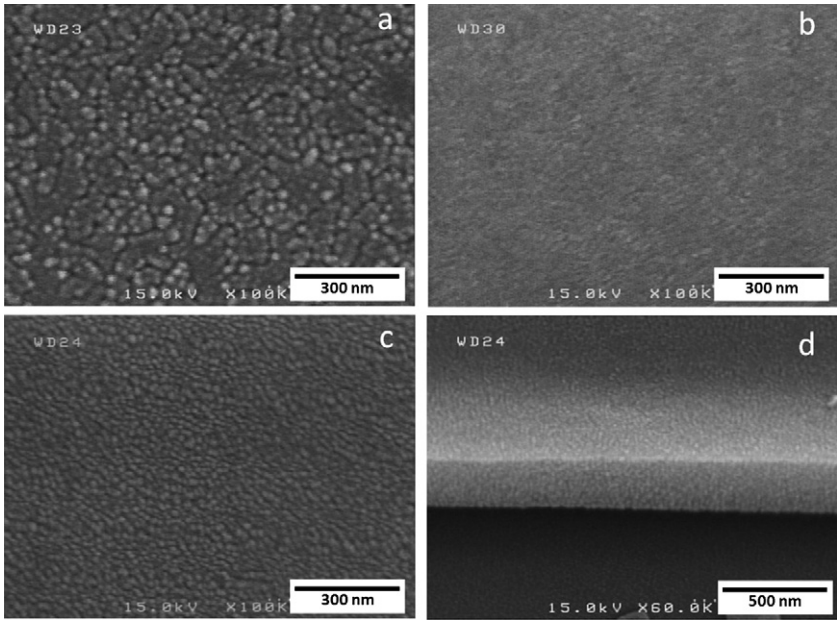

Fig. 4. FESEM micrographs of (a) MeOH, (b) EtOH, (c) 1PrOH, and (d) cross section view of 1PrOH sample calcined at 450 °C.

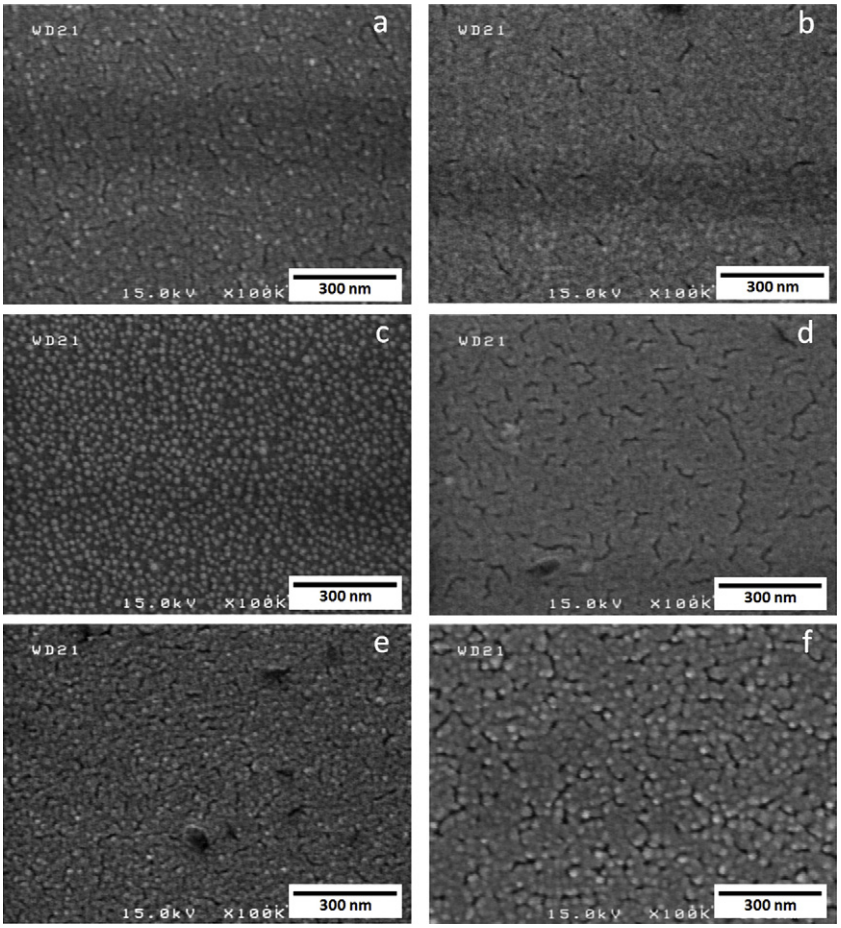

Fig. 5. FESEM micrographs of (a) EtOH/2PrOH, (b) MeOH/2PrOH, (c) MeOH/1PrOH, (d) MeOH/EtOH, (e) 1PrOH/2PrOH, and (f) EtOH/1PrOH samples calcined at 450 °C.

3.3. Thermal analysis

Fig. 6 shows DSC/TG curves of samples with individual solvents of MeOH, EtOH, 1PrOH, 2PrOH. In MeOH and EtOH samples, the weight loss mostly occurs below 300 °C, while in 2PrOH sample the weight loss continues to 400 °C. In these samples the weight loss can be divided into three temperature regions below 180 °C, which might be the result of evaporation of water and solvent, between 180 and 250 °C, which is attributed to thermal decomposition of remnant organic solvents, and between 250 and 350 °C, which is probably due to the combustion of residual alkoxy groups and carbonization of organic constituents. The endothermic peaks in DSC curves in first region ascribe the evaporation and organic loss. Two exothermic peaks have been observed in the range of 250–380 °C for all samples. These peaks could be related to the carbonization and combustion of organic substances, respectively. Very low intensity exothermic peak at 469 °C in MeOH may be due to the crystallization temperature of anatase TiO_2 phase. This peak shifts to lower temperature (450 °C) in EtOH, while it shifts to 550 °C in 2PrOH. It is believed that in 1PrOH sample the self-propagating combustion reaction happened which resulted in a very high exothermic peak in DSC curve and loss of powder from crucible. In first stage the weight loss of the sample is about 12% of its original weight. In second stage the sample weight loss is about 6%, and the lowest weight loss of about 2% occurs in third stage. The overall weight loss for MeOH, EtOH, and 2PrOH is about 23%, 37%, and 20%, respectively.

3.4. UV/vis analysis

The UV/vis transmittance spectra of the 10-layer calcined thin films with solvents of MeOH, EtOH, 1PrOH and 1BuOH were compared in Fig. 7a. It could be seen that all films have the transmittance of higher than 80% in visible region with oscillation and very strong absorption at around band gap. The optical band gap of the films was calculated using Tauc equation [30]:

$$\alpha h\nu = k(h\nu - E_g)^n \quad (1)$$

where α is the absorption coefficient, k is constant, $h\nu$ is the photon energy in eV, and the value of n can be 1/2 for allowed direct, 2 for allowed indirect, 3 for forbidden direct, and 3/2 for forbidden indirect transitions [31]. The band gap was estimated by extrapolating the straight line portion of the $(\alpha h\nu)^n$ vs. $h\nu$ plot (Fig. 7b). TiO_2 has many different transitions in polarized light and the lowest transitions are direct transitions of $X_1 \rightarrow X_1$ (3.45 eV, E⊥C) and $X_2 \rightarrow X_1$ (3.59 eV, E∥C) and

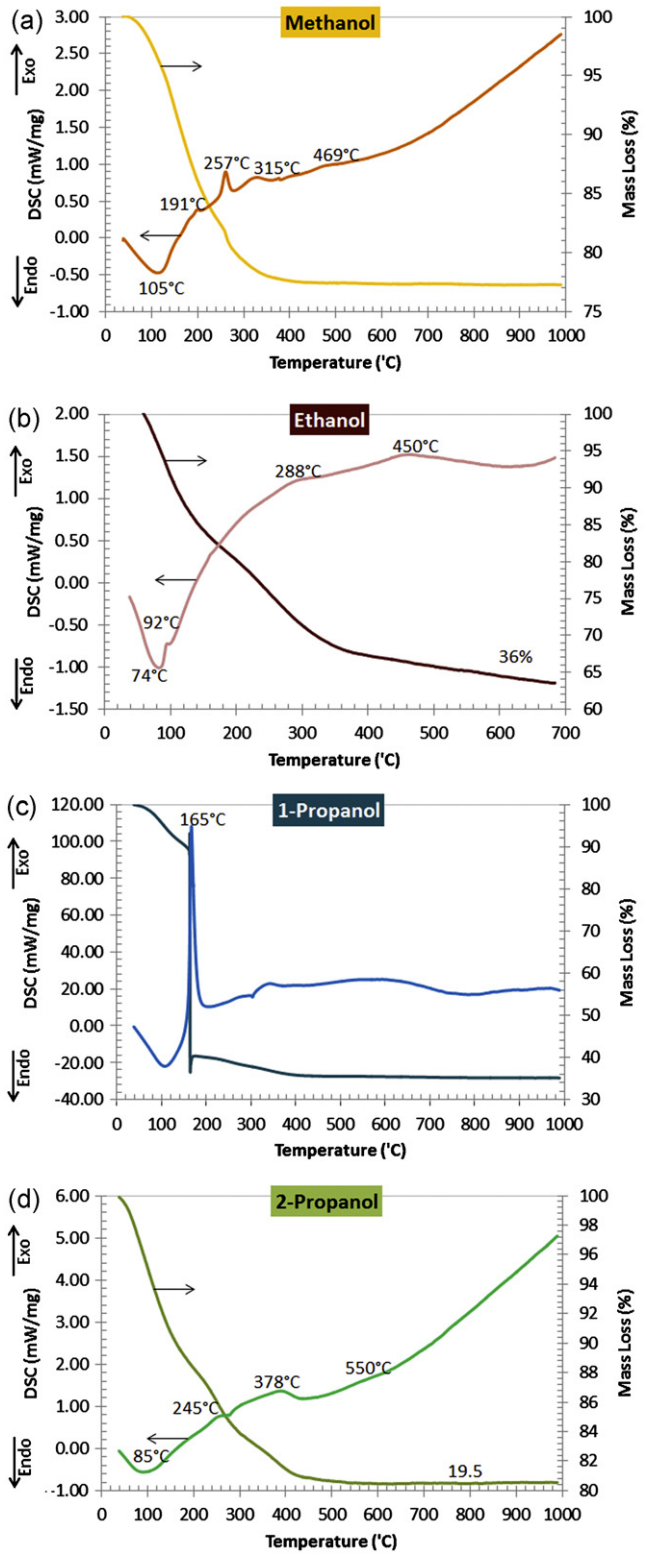

Fig. 6. DSC/TG curves for (a) MeOH, (b) EtOH, (c) 1PrOH, and (d) 2PrOH samples.

indirect transitions of $X_1 \rightarrow \Gamma_1$ (2.91 eV, E⊥C) and $X_2 \rightarrow \Gamma_1$ (3.05 eV rutile, 3.14 eV anatase, E||C) [11,32,33]. All films show the direct transition at around 3.4 eV which is matched with the $X_1 \rightarrow X_1$ transition (the stoichiometric band gap of TiO_2). The indirect transition of anatase TiO_2 (nonstoichiometric band gap)

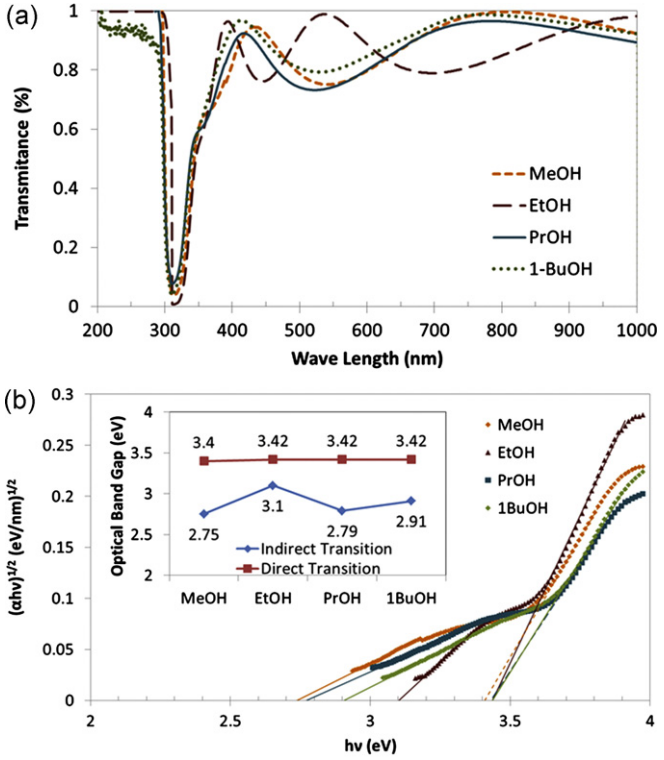

Fig. 7. (a) UV/vis transmittance spectra and (b) Tauc plots of the 10-layer calcined thin films with solvent of MeOH, EtOH, 1PrOH, and 1BuOH. Inset (b) calculated values of direct and indirect band gaps.

is about 3.14–3.2 eV and shows itself just in the case of EtOH. In MeOH, 1PrOH and 1BuOH samples indirect transitions cannot be correctly detected and shifted to lower energies due to the high extinction coefficient in strong absorption region (blue part of spectrum) and interference of the refractive index oscillation with indirect transition.

Fig. 8a shows the optical transmittance of 10-layer mixed solvent samples calcined at 450 °C. The same as individual solvents, all mixed solvent samples show transparency more than 80% in visible region and optical band gap at UV region. The thickness of the films, crystallinity, porosity, composition (rutile phase percentage), and number of layers are affected by the mixed solvent. Therefore, the oscillation of the transmittance in visible region is changed for mixed solvent samples. As the absorption coefficient of free carriers is very low and the energy range of phonons is far from the investigated energy range; the contributions of free carriers and phonons to the refractive index can be neglected. Fig. 8b illustrates the Tauc plot for mixed solvent samples. As in the individual solvents, these samples show the direct transition at around 3.4 eV and the indirect transition at around 3.2 eV which in some samples (MeOH/1PrOH, 1PrOH/2PrOH, and EtOH/1PrOH) this transition could not be correctly detected because of the interference of refractive index oscillation in strongly absorption region with indirect transition. However, the direct transition for MeOH/EtOH sample could not be extracted. Many structural, morphological, and optical inter-related parameters could affect the band gap of thin films. Crystallinity, thickness, morphology, and packing density should be considered

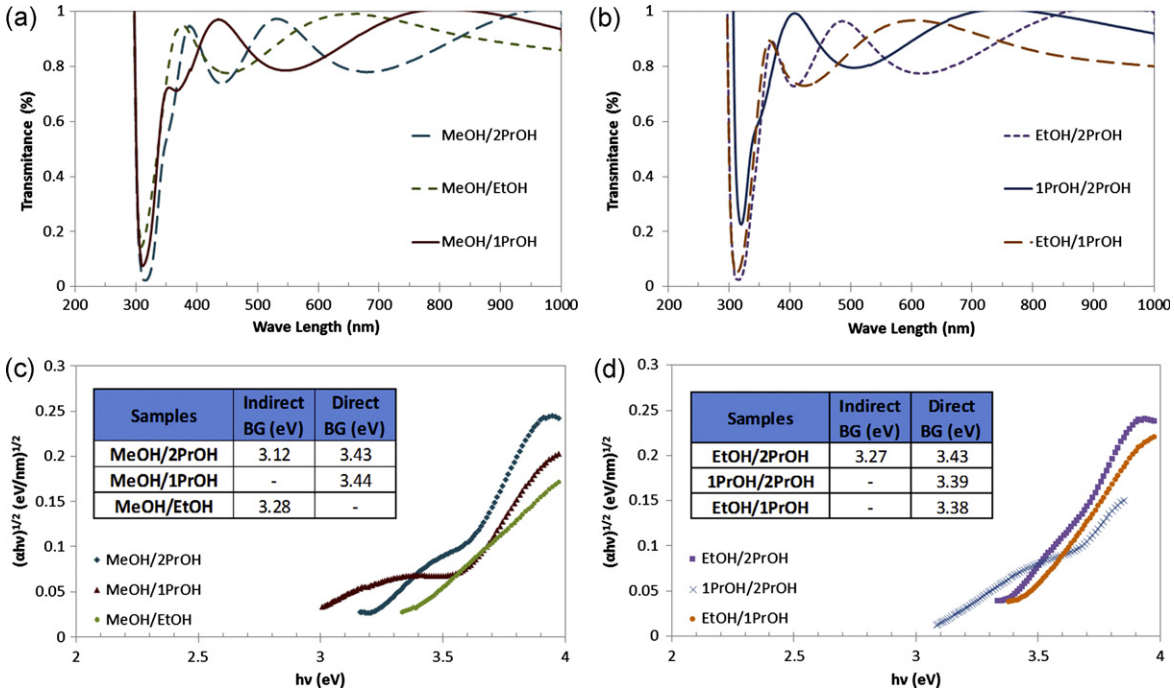

Fig. 8. (a) and (b) Optical transmittance and (c) and (d) Tauc plots of 10-layer mixed solvent samples calcined at 450 °C. Inset (c) and (d) are calculated values of direct and indirect band gaps.

concerning the band gap of MeOH/EtOH sample. As the packing densities for all samples are slightly the same, other parameters such as crystallinity which is low for this sample, thickness which is also low, and morphology which shows inter-diffused grains with interconnected pores in between, should be taken into account. Since the only samples with both low crystallinity and low thickness are MeOH/EtOH and 1PrOH/2PrOH, two hypotheses are raised for disappearance of direct transition in MeOH/EtOH: (1) the low crystallinity and thickness of this sample besides the different morphology cause disappearance of direct transition; and (2) two low boiling point solvents cause the direct transition value narrowed and shifted to lower energies by generating defect-derived shallow levels in band gap of anatase. These hypotheses are still under debate and need more consideration.

The refractive index of the films was calculated using the modified envelope method. In this method the refractive index of the thin film could be calculated using the oscillation of the transmittance spectra [34–36].

$$n = \left(N + \sqrt{(N^2 - n_s^2)}\right)^{1/2} \tag{2}$$

where

$$N = \frac{1}{2}(1 + n_s^2) + \frac{8n_s^2}{(n_s + 1)^2}\left(\frac{T_M - T_m}{T_M T_m}\right) \tag{3}$$

The T_M and T_m are the maxima and minima of the envelope in transmittance spectra, and n_s are the refractive index of the glass substrate which can be calculated from the transmittance of the glass spectra:

$$n_s = \frac{1}{T_s} + \left(\frac{1}{T_s^2} - 1\right)^{1/2} \tag{4}$$

The refractive index, approximate thickness, and packing density of the films are shown in Table 3. The observed

Table 3
Refractive indices, calculated thicknesses, observed thicknesses, and packing densities of the films.

Sample	Refractive index	Calculated thickness (nm)	Observed thickness (nm)	Packing density
MeOH	2.15 ± 0.11	447 ± 53	410 ± 10	0.78 ± 0.08
EtOH	2.06 ± 0.10	700 ± 60	600 ± 20	0.72 ± 0.07
PrOH	2.13 ± 0.11	496 ± 45	480 ± 10	0.76 ± 0.08
1BuOH	2.02 ± 0.10	525 ± 47	460 ± 10	0.69 ± 0.07
EtOH/2PrOH	2.03 ± 0.10	695 ± 58	640 ± 20	0.70 ± 0.07
MeOH/2PrOH	2.03 ± 0.10	808 ± 72	710 ± 20	0.70 ± 0.07
MeOH/1PrOH	2.08 ± 0.10	523 ± 45	450 ± 10	0.74 ± 0.07
MeOH/EtOH	2.10 ± 0.11	385 ± 40	370 ± 10	0.75 ± 0.08
1PrOH/2PrOH	2.06 ± 0.10	438 ± 42	400 ± 10	0.72 ± 0.07
EtOH/1PrOH	2.13 ± 0.11	359 ± 35	320 ± 10	0.76 ± 0.08

thickness values from FESEM cross sectional images were also compared in this table and confirmed the trends of calculated values. The volume fraction or packing density of the films (f) could be achieved via:

$$f\frac{n_b^2-n^2}{n_b^2+2n^2}+(1-f)\frac{1-n^2}{1+2n^2}=0 \quad (5)$$

where n_b is the refractive index of the bulk material and n is the measured refractive index [29]. It was found that the refractive index in the case of ethanol as a solvent was smaller than methanol or propanol. The origin of refractive index has come from the difference between frequency of the radiation and resonant frequency of an electron bound in an atom. However, in calculating refractive index from transmittance spectra, the refractive index is the function of thickness, density, purity (here means rutile to anatase ratio), dopant and defect concentration, porosity, lattice distortion, interfaces in multilayer samples, substrate refractive index, extinction coefficient, and wavelength. The faster the gel time of the sol, the thicker the film thickness, and as a result the higher refractive index could be observed. The ethanol sample shows the highest thickness between individual solvent samples which is due to the shortest gel time of this sample, which causes faster hydrolysis and condensation in thin film formation process, higher viscosity, and thicker film. In addition, the higher refractive index in ethanol sample could be related to some extent to the formation of rutile in this sample. The methanol sample causes lower thickness due to its lower boiling point than propanol. On the other hand, the 1BuOH sample has very high viscosity and boiling point. Upon film formation, there is a competition between solvent drying and sol spreading (and as a result gel formation) on the substrate. Consequently, the thickness of the 1BuOH is higher than MeOH and PrOH but lower than EtOH. Also, the packing density of this sample is the lowest. Therefore, the refractive index shows very low amount.

Film packing which relates to the porosity of the film, number of layers, the disordered space between each layer, and also surface roughness, shows low values in ethanol. It could be seen that the lower the film viscosity is, the thinner and the denser the film is. Among the four individual solvents, the film with ethanol shows the highest thickness, which is mainly affected by gel time of the sol. With decreasing the gel time of the sol, the viscosity rises and causes a thicker film. Besides gel time and viscosity, other interrelated parameters such as the boiling point of the solvent, possible complexes, concentration, water content, pH, and spin coating parameters could affect the thickness of the films. Methanol and propanol show lower thickness than ethanol due to the more complicated complexes which result in higher gel time and hence lower viscosity. On the other hand, methanol sample has the lower thickness than propanol even with lower boiling point.

In mixed solvent samples, the refractive index is in the range of 2.03–2.15. Also, all the mixed solvent samples demonstrate more than 70% packing and the highest packing was achieved in EtOH/PrOH sample. All the systems which contain the 2PrOH as one solvent component formed the film with high thickness. The 2PrOH can easily form the monomeric complex with alkoxide for its similarities with alkoxide ligand (H_3C–$CH(O)$–CH_3) and has fast hydrolysis and condensation reaction rates due to its low steric hindrance. This leads to the higher viscosity and faster gel time during the film deposition which result in higher thickness. On the other hand, all other samples contain 2PrOH beside other solvents for their alcohol exchange reaction as follows:

$$Ti(OC_3H_7)_4 + xR'(OH) \rightarrow Ti(OC_3H_7)_{4-x}(OR')_x + xC_3H_7OH \quad (6)$$

where R′ is the alkyl group. However, the amount of 2PrOH is very small because of the small amount of alkoxide in prepared sols. In 1PrOH/2PrOH sample, the gel time is long enough to form a very thin film, but existence of 2PrOH promotes the formation of very tiny particles which cause the milky sol after 2 days and opaque gel after 5 days which affects the thickness of the film during film preparation. The alcohol exchange rate decreases as MeOH > EtOH > 2PrOH > 1PrOH > 1BuOH which confirms that in MeOH/1PrOH sample, the difference in alcohol exchange rate between two components is noticeable compare to the MeOH/EtOH. This leads to the methoxy based complexes. In addition, the existence of very small amount of water in MeOH formed tiny particles in sol. This and aforementioned statement causes translucent sol after three days. These particles could be observed in SEM micrograph of this sample. The EtOH/1PrOH sample shows the longest gel time of more than eight days and the lowest thickness of about 360 nm for more similar properties of the solvents in terms of boiling point, dipole moment, molecular weight, and alcohol exchange rate. From the steric hindrance point of view, oligomerization of 2-propoxy with short length group of methoxy causes low steric hindrance and fast hydrolysis. 2-Propoxy oligomerization in solvents contains 2PrOH leads to monomeric hindrance. Ethoxy group is more reactive than 1-propoxy group which describes the faster gel time of EtOH compare to 1PrOH as one component solvents. From the dipole moment point of view, the decrease in dipole moment leads to larger length over which the charged species affected their surrounding species. Thus, electrostatic stabilization could be better in lower dipole moment solvents.

4. Conclusions

Transparent TiO_2 thin films with slightly different optoelectrical properties have been prepared on glass substrates from alkoxide solution with different individual solvents of MeOH, EtOH, 1PrOH, 2PrOH, 1BuOH, 2BuOH and tBuOH as well as mixed solvents of EtOH/2PrOH, MeOH/2PrOH, MeOH/1PrOH, MeOH/EtOH, 1PrOH/2PrOH, and EtOH/1PrOH. It was found that the sol stability and transparency of 2PrOH, 2BuOH and tBuOH sols were not suitable for film formation. On the other hand, MeOH, 1PrOH and 1BuOH show great sol stability and gel time which resulted in a very high quality films. Although the anatase phase was the major crystalline phase in all samples, very low amount of the rutile phase formed in EtOH and 1PrOH, and mixing the solvent strongly reduces the rutile formation. In addition, FESEM micrographs confirmed

that very small particles formed on films with MeOH as a solvent. The packing and morphology of the films related to the viscosity and boiling point of the sols and show different morphologies. Interestingly, all the films show different solvent related optical oscillation behavior in visible region. It was found that viscosity, gel time, boiling point, possible complexes, dipole moment, and chain length of the solvent could efficiently affect the packing density, lattice distortion, interfaces, thickness, optical band gap, refractive index, and extinction coefficient. Mixing solvents leads to the films with desired morphologies, band gaps, refractive indices, and also crystalline phases.

Acknowledgment

The authors would like to thank Iran Nanotechnology Initiative council for partially supporting this research.

References

[1] D.A. Tryk, A. Fujishima, K. Honda, Recent topics in photoelectrochemistry: achievements and future prospects, Electrochimica Acta 45 (2000) 2363–2376.
[2] M. Grätzel, Photoelectrochemical cells, Nature 414 (2001) 338–344.
[3] P.V. Kamat, Quantum dot solar cells. Semiconductor nanocrystals as light harvesters, Journal of Physical Chemistry C 112 (2008) 18737–18753.
[4] M. Ferroni, V. Guidi, G. Martinelli, G. Faglia, P. Nelli, G. Sberveglieri, Characterization of a nanosized TiO_2 gas sensor, Nanostructured Materials 7 (1996) 709–718.
[5] H. Kostlin, G. Frank, G. Hebbinghaus, H. Auding, K. Denissen, Optical filters on linear halogen-lamps prepared by dip-coating, Journal of Non-Crystalline Solids 218 (1997) 347–353.
[6] X. Chen, S.S. Mao, Titanium dioxide nanomaterials: synthesis, properties, modifications, and applications, Chemical Reviews 107 (2007) 2891–2959.
[7] K.A. Vorotilov, E.V. Orlova, V.I. Petrovsky, Sol–gel TiO_2 films on silicon substrates, Thin Solid Films 207 (1992) 180–184.
[8] A.K. Hassan, N.B. Chaure, A.K. Ray, A.V. Nabok, S. Habesch, Structural and electrical studies on sol–gel derived spun TiO_2 thin films, Journal of Physics D: Applied Physics 36 (2003) 1120–1126.
[9] Y. Takahashi, Y. Matsuoka, Dip-coating of TiO_2 films using a sol derived from $Ti(O\text{-}i\text{-}Pr)_4$-diethanolamine-$H_2O$-i-PrOH system, Journal of Material Science 23 (1988) 2259–2266.
[10] A. Fujishima, X. Zhang, D.A. Tryk, TiO_2 photocatalysis and related surface phenomena, Surface Science Reports 63 (2008) 515–582.
[11] R. Asahi, Y. Taga, W. Mannstadt, A. Freeman, Electronic and optical properties of anatase TiO_2, Physical Review B: Solid State 61 (2000) 7459–7465.
[12] A.L. Linsebigler, G. Lu, J.T. Yates, Photocatalysis on TiO_2 surfaces: principles, mechanisms, and selected results, Chemical Reviews 95 (1995) 735–758.
[13] M.H. Habibi, N. Talebian, J.H. Choi, The effect of annealing on photocatalytic properties of nanostructured titanium dioxide thin films, Dyes and Pigments 73 (2007) 103–110.
[14] C. Yang, H. Fan, Y. Xi, J. Chen, Z. Li, Effects of depositing temperatures on structure and optical properties of TiO_2 film deposited by ion beam assisted electron beam evaporation, Applied Surface Science 254 (2008) 2685–2689.
[15] T. Viseu, M.R. Ferreira, M.C. Isabel, Morphological characterization of TiO_2 thin films, Vacuum 52 (1999) 115–120.
[16] C.J. Brinker, A.J. Hurd, P.R. Schunk, G.C. Frye, C.S. Ashley, Review of sol–gel thin film formation, Journal of Non-Crystalline Solids 147 (1992) 424–436.
[17] C.Y.W. Lin, D. Channei, P. Koshy, A. Nakaruk, C.C. Sorrell, Effect of Fe doping on TiO_2 films prepared by spin coating, Ceramics International 38 (2012) 3943–4946.
[18] J. Tian, L. Chen, J. Dai, X. Wang, Y. Yin, P. Wu, Preparation and characterization of TiO_2, ZnO, and TiO_2/ZnO nanofilms via sol–gel process, Ceramics International 35 (2009) 2261–2270.
[19] R. Janisch, P. Gopal, N.A. Spaldin, Transition metal doped TiO_2 and ZnO: present status of the field, Journal of Physics: Condensed Matter 17 (2005) 657–689.
[20] J.J. Wu, C.C. Yu, Aligned TiO_2 nanorods and nanowalls, Journal of Physical Chemistry B 108 (2004) 3377–3379.
[21] S. Liu, K. Huang, Straightforward fabrication of highly ordered TiO_2 nanowire arrays in AAM on aluminum substrate, Solar Energy Materials and Solar Cells 85 (2004) 125–131.
[22] Y. Suda, H. Kawasaki, T. Ueda, T. Ohshima, Preparation of nitrogen-doped titanium oxide thin film using a PLD method as parameters of target material and nitrogen concentration ratio in nitrogen/oxygen gas mixture, Thin Solid Films 475 (2005) 337–341.
[23] I. Oja, A. Mere, M. Krunks, R. Nisumaa, C.H. Solterbeck, M. Es-Souni, Structural and electrical characterization of TiO_2 films grown by spray pyrolysis, Thin Solid Films 515 (2006) 674–677.
[24] N.R. Mathews, E.R. Morales, M.A. Cortes-Jacome, J.A. Toledo Antonio, TiO_2 thin films – influence of annealing temperature on structural, optical and photocatalytic properties, Solar Energy 83 (2009) 1499–1508.
[25] L. Hu, T. Yoko, H. Kozuka, S. Sakka, Effects of solvent on properties of sol–gel derived TiO_2 coating films, Thin Solid Films 219 (1992) 18–23.
[26] Powder Diffraction File, Joint Committee on Powder Diffraction Standards, ASTM, Philadelphia, PA, 1969, Card 21-1272.
[27] Powder Diffraction File, Joint Committee on Powder Diffraction Standards, ASTM, Philadelphia, PA, 1969, Card 21-1276.
[28] U. Diebold, The surface science of titanium dioxide, Surface Science Reports 48 (2003) 53–229.
[29] J.I. Langford, A.J.C. Wilson, Scherer after sixty years: a survey and some new results in the determination of crystallite size, Journal of Applied Crystallography 11 (1978) 102–113.
[30] J. Tauc, Optical properties and electronic structure of amorphous Ge and Si, Materials Research Bulletin 3 (1968) 37–46.
[31] M.M. Hasan, A.S.M.A. Haseeb, R. Saidur, H.H. Masjuki, Effects of annealing treatment on optical properties of anatase TiO_2 thin films, World Academy of Science, Engineering and Technology 40 (2008) 221–225.
[32] N. Daude, C. Gout, C. Jouanin, Electronic band structure of titanium dioxide, Physical Review B: Solid State 15 (1977) 3229–3235.
[33] S.D. Mo, W.Y. Ching, Electronic and optical properties of three phases of titanium dioxide: rutile, anatase and brookite, Physical Review B: Solid State 51 (1995) 13023–13032.
[34] C.H. Peng, S.B. Desu, Modified envelope method for obtaining optical properties of weakly absorbing thin films and its application to thin films of $Pb(Zr,Ti)O_3$ solid solutions, Journal of the American Ceramic Society 77 (1994) 929–938.
[35] R. Swanepoel, Determination of the thickness and optical constants of amorphous silicon, Journal of Physics E: Scientific Instruments 16 (1983) 1214–1222.
[36] J.C. Manifacier, J. Gasiot, J.P. Fillard, A simple method for the determination of the optical constants n, k and the thickness of a weakly absorbing thin film, Journal of Physics E: Scientific Instruments 9 (1976) 1002–1004.